Composites Communications 51 (2024) 102048

Contents lists available at ScienceDirect

Composites Communications

journal homepage: www.elsevier.com/locate/coco

Electrospun graphene oxide/polymeric nanocomposites for eardrum replacements

Mario Milazzo [a,b,*], Serena Danti [a,b], Pieter Livens [c], Joris Dirckx [c], Roberto Scaffaro [b,d,**], Michele Gammino [d]

[a] Department of Civil and Industrial Engineering, University of Pisa, Largo L. Lazzarino 2, 56126, Pisa, Italy
[b] Consorzio Interuniversitario Nazionale per la Scienza e Tecnologia dei Materiali (INSTM), via Giusti 9, 50121, Florence, Italy
[c] Laboratory of Biomedical Physics (BIMEF), University of Antwerp, Groenenborgerlaan 171, Antwerp, 2020, Belgium
[d] Dipartimento di Ingegneria, Università di Palermo, Viale delle Scienze, 90128, Palermo, Italy

ARTICLE INFO

Keywords:
Finite element modeling
Mechanical characterization
Biomaterials
Acoustics

ABSTRACT

The development of structures and devices with enhanced acousto-mechanical properties is a topic of interest in engineering, especially in the biomedical field. A case study is the reconstruction of the tympanic membrane after partial or complete damage, such as from chronic suppurative otitis media, which is the leading cause of infectious diseases in children. In this work, we developed graphene-oxide (GO) nanocomposite polymeric scaffolds fabricated via electrospinning to assess their potential suitability as substitutes of the eardrum. To evaluate the structural influence of GO on the fibrous mesh, we performed a characterization in terms of wettability, mechanical properties, and surface morphology. Moreover, a finite-element model of the middle ear was employed to assess the acousto-mechanical behavior of the eardrum upon application of the developed scaffolds. We observed that GO influenced the morphology of the fibrous scaffolds by increasing the mean diameter of the fibers, their stiffness and strength, while decreasing the water contact angle, thus making the structures more hydrophilic. From the acoustic standpoint, the simulations showed that GO does not significantly affect sound transmission, except for PVDF-based structures, for which GO slightly improves the behavior only up to 2 kHz, but with a suboptimal performance at higher frequencies. Our results open to the development of fibrous nanocomposite polymeric scaffolds with an enhanced acoustic behavior for structural applications not limited to bioengineering.

1. Introduction

Acoustic transmission and dissipation are key properties that are relevant in many different fields, from civil engineering and automotive to bioengineering, since they can, for instance, improve people's comfort and well-being [1]. Within the biomedical field, the latest statistics from the World Health Organization showed that about 430 million people worldwide suffer from disabling hearing loss, a trend that is estimated to rise to over 700 million people by 2050 [2]. To deal with this challenge, researchers have developed engineered solutions to treat hearing deficiencies of the sensory cell function of the inner ear (i.e., sensorineural hearing loss), or transmissive dysfunctions of the middle ear structures, such as the tympanic membrane (TM) and the ossicular chain (i.e., conductive hearing loss). In particular, the TM, (or eardrum), is devoted to collect sounds from the outer ear and to selectively transmit pressure waves to the middle ear [3–5], and its recovering after traumas, pathologies, or insertion of foreign bodies still represents a challenge [6–8]. The TM damage poses, in fact, an intriguing case study, since it is made of a layered structure with an anisotropic orientation of collagenous fibers, covered by two different epithelia, leading to a non-uniform construct whose thickness ranges between 30 and 150 μm. The quest for optimal eardrum replacements is driven by a set of crucial criteria, which try to accomplish the complex physiological anatomy and functional characteristics of the TM, including mechanical strength, to endure the dynamic and potentially harsh conditions of the ear canal, and specific acoustic characteristics to restore or maintain the critical role of TM in sound transmission [9]. Many clinical and bioengineering approaches have been developed to create adequate TM replacements.

* Corresponding author. Department of Civil and Industrial Engineering, University of Pisa, Largo L. Lazzarino 2, 56126, Pisa, Italy.
** Corresponding author. Dipartimento di Ingegneria, Università di Palermo, Viale delle Scienze, 90128 Palermo, Italy.
E-mail addresses: mario.milazzo@unipi.it (M. Milazzo), roberto.scaffaro@unipa.it (R. Scaffaro).

https://doi.org/10.1016/j.coco.2024.102048
Received 11 July 2024; Received in revised form 13 August 2024; Accepted 17 August 2024
Available online 19 August 2024

Among them, the gold standard surgical solutions consist in using autologous materials [10–12] (i.e., temporal fascia, cartilage) as patches or complete substitutes of the native tissue [11,13,14]. Traditional tissue replacements present issues such as curling, adhesion post-surgery, and inadequate resistance to infections, albeit avoiding rejection reactions [10,15]. On the other hand, tissues like tragus cartilage are frequently employed for repairing large perforations due to its greater mechanical strength, but its thickness often leads to increased acoustic impedance and subsequent suboptimal hearing [16,17]. Therefore, it is the combination of the physical and mechanical properties of the constituent material with the morphology of the constructs that leads to a specific acoustic impedance and, therefore, to the specific acoustic behavior.

While past research efforts have predominantly focused on enhancing specific regenerative attributes, there is a growing recognition of the need for biomaterials encompassing a broad spectrum of superior acousto-mechanical qualities. Natural polymers, structurally and compositionally similar to the extracellular matrix have emerged as promising candidates for TM scaffolds: calcium alginate [18,19], silk fibroin [18,20], and chitosan [10] have been explored to create TM substitutes; however, they generally show limited mechanical properties and acoustic performance [21]. Synthetic polymers, in contrast, are characterized by significant mechanical properties and stability. In particular, materials like poly (lactic acid) (PLA) [22–24], poly (lactic-*co*-glycolic acid) (PLGA) [25], polycaprolactone (PCL) [26–28], and poly (vinylidene fluoride-*co*-hexafluoroprolylene) (PVDF-*co*-HFP) [29–32] have been extensively employed in tissue engineering, and are good candidates for eardrum replacements.

From the manufacturing standpoint, electrospinning stands out as an ideal technique for fabricating porous polymeric scaffolds with high specific surface area, porosity and tunable mechanical properties [33,34]. The versatility of the electrospinning process has been demonstrated in applications beyond bioengineering [16,17], such as catalysis [35], water remediation [26,29,36], smart food packaging [37], and drug delivery [38].

For instance, Mota et al. developed a multilayered construct that mimics the complex anisotropic arrangement of collagen through a synergistic manufacturing approach involving both extrusion-based printing and electrospinning, using poly (ethylene oxide terephthalate)- poly (butylene terephthalate) (PEOT-PBT) [39]. Subsequent studies have investigated the role of 3D printed geometries, showing a geometrical dependency of their mechanical and acoustical responses, in which radially aligned fibers were observed to have a more prominent effect compared to their circumferential counterparts [40].

Benecke et al., on the other hand, developed eardrum-like implants via electrospinning using PCL and silk fibroin, demonstrating the technical feasibility to create complex constructs finely tunable to match the expected acoustic performance [41].

To improve and tune the mechanical properties of electrospun fiber meshes, researchers have explored the possibility of employing ceramic particles as nanofillers. Graphene and its derivatives, and in particular graphene oxide (GO), have recently gained interest because of their ability to tune specific physico-chemical characteristics from optical, electrical, mechanical, antimicrobial to biocompatibility properties [42–44].

Recent examples of GO employment in the biomedical field were reported for mechanically reinforcing poly-L-lactic acid (PLLA) for bone replacements either in combination with hydroxyapatite [45] or molybdenum disulphide (MoS_2) [46]. A different approach was employed by Feng et al. that used PLLA chains grafted onto graphene oxide (PLLA-grafted GO) by ring-opening polymerization reaction, in order to improve the interfacial interaction in PLLA-grafted GO/PGA scaffolds fabricated by selective laser sintering. This approach led to increased tensile/compressive strengths compared to PLLA/PGA structures, without any biological drawback in terms of cytocompatibility, and cell adhesion, migration, and proliferation [47].

To the authors' knowledge, the employment of GO-based polymeric nanocomposites as constitutive materials for acoustic applications has not been discussed in literature so far. Therefore, this work aims to develop and characterize electrospun GO-based polymeric membranes as potential candidates for eardrum tissue replacements. Specifically, we assessed the influence of GO on the physico-chemical, mechanical, and acousto-mechanical behaviors of the electrospun structures by exploiting finite-element simulations mimicking the actual application of such materials as constituents of the eardrum.

Our results on integrating the unique properties of nanomaterials in polymers hold significant potential for lightweight devices in the biomedical field. Moreover, the convergence of materials research in acoustics and tissue engineering and advancements in nanomaterial integration opens new avenues for developing multifunctional materials with enhanced acousto-mechanical properties and tailored morphologies, with applications not limited to the bioengineering field.

1.1. Materials and methods

1.1.1. Polymers

We purchased from NatureWorks (Minneapolis, Mn, USA): the Polylactic acid (PLA) (2003D grade) with density of 1.25 g/cm^3, melt flow index of 6 g/10 min, and D-lactic acid monomer content of 4.3 %; Polycaprolactone (PCL) with molecular weight (M_n) of 80 kDa, polydispersity index (M_w/M_n) of less than 2, density of 1.14 g/cm^3, and melting temperature of 60 °C; 75:25 Poly (lactic-*co*-glycolic acid) (PLGA) with molecular weight (M_w) of 100 kDa.

PVDF-co-HFP, later referred to PVDF-HFP, was graciously provided by CTS Europe (Altavilla Vicentina (VI), Italy). This elastomeric thermoplastic fluorinated copolymer possesses a M_w of 4×10^5 g/mol and 1.77 g/cm^3 density.

The employed solvents, namely dichloromethane (DCM), ethanol (EtOH), acetone (Ac), chloroform (CF), 1,1,1,3,3,3-hexafluoro-2-propanol (HFIP), and deionized distilled water (DDW), and hydrochloric acid (HCl) were purchased from Sigma-Aldrich (Merck KGaA, St. Louis, MO, USA). All reactants are of ACS grade and used without further treatment.

1.1.2. Synthesis of graphene oxide

Graphene Oxide (GO) (lateral size <45 μm, thickness = 0.7–0.8 nm, C/O ratio = 1.1, density = 1.76 g/cm^3) was synthesized starting from natural graphite by using Tour's method [48] according to our previous works [49–52]. Briefly, graphite powder (10 g) and $KMnO_4$ (60 g) were added to the H_2SO_4/H_3PO_4 (9:1 b y volume) mixture (900 mL) and kept for 16 h under continuous stirring. After that, the reaction was quenched with H_2O_2 (30 w% in H_2O) and ice. Several centrifugations were carried out with HCl, H_2O, and EtOH for the workup.

1.1.3. Preparation of the electrospinning solutions

To prepare the solutions for electrospinning, each PLA, PCL, PLGA, and PVDF-HFP sample was added at 10 w% to 20 mL of solvent or solvent mixtures, as detailed in Table 1, referring to previous works [29,53].

GO nanoparticles were initially dispersed in 20 mL of different solvents (Table 1) and later completely dissolved through three cycles of ultrasonication for 2 h, followed by stirring for 30 min. Cold water was intermittently added to the ultrasonic bath to keep a constant temperature.

Each polymeric solution was then added to the GO/solvent-solvent mixture and dispersed under continuous magnetic stirring overnight at room temperature, reaching a composition of 10 w% of polymer in the specific solvent, as outlined in Table 1, the amount of GO was selected to produce a series of nanocomposite PCL/GO, PLA/GO, PLGA/GO, PVDF-HFP/GO electrospun structures with GO concentrations up to 1.0 w%.

1.1.4. Electrospinning process

A conventional electrospinning equipment (Linari Engineering s. r.l., Pisa, Italy) was employed to prepare nanofibers of pure polymer

Table 1
Solution formulations and main parameters for the electrospinning manufacturing process.

	Sample	Solvent	Solvent ratio	Polymer/GO (w%/w%)	V (kV)	Collector distance/speed (cm/rpm)
Neat polymers	PLA	CF:Ac	2:1	10	15	15/50
	PCL	DCM:EtOH	3:1		18	
	PVDF	Ac	–		17	
	PLGA	HFIP	–		17	
Nano-composites	PLA/GO	CF:Ac	2:1	9/1	15	15/50
	PCL/GO	DCM:EtOH	3:1		18	
	PLGA/GO	HFIP	–		17	
	PVDF/GO	Ac	–		17	

matrices, as well as their composites, namely PCL/GO, PLA/GO, PLGA/GO, and PVDF-HFP/GO composites. Each solution was loaded into a 10-mL glass syringe with a 19G stainless steel needle. Electrospinning was performed under constant parameters: flow rate of 3 mL/h, distance of 15 cm between the needle tip and the collector, specific high voltages (as determined in previous works [29,53,54] and reported in Table 1), temperature set at 25 °C, and relative humidity set at 40 %. The resulting nanofibers were collected on a grounded rotary drum (diameter 100 mm) and deposited on an aluminum foil. The rotary drum run at 50 rpm, and the collection time was 120 min to achieve structures with a thickness of approximately 50 μm. Subsequently, the collected fiber meshes were air-dried for at least 2 days under a fume hood to eliminate any residual solvents.

1.1.5. Characterization of the electrospun membranes

1.1.5.1. Morphological and physical properties. The morphology of the polymeric and nanocomposite membranes was evaluated by Scanning Electron Microscopy (SEM) (Phenom ProX, Phenom-World, Thermo Fisher Scientific, Waltham, MA, USA). The samples were attached on an aluminum stub using an adhesive carbon tape and then sputtered with gold (Sputtering Scancoat Six, Edwards) for 90 s in an Argon atmosphere.

Image analysis, performed by ImageJ 8 open-source software (ImageJ, NIH, USA https://imagej.nih.gov/ij/download.html) equipped with the Diameter J plug-in, was used to measure the meshes' fiber diameter distribution and pore diameters [55–57].

A Thermo Pycnomatic Helium Pycnometer (Pycnomatic ATC, Thermo Fisher Scientific, Waltham, MA, USA) with 99.99 % pure Helium was used in the characterization, and measurements were repeated five times for each sample at 20 °C.

The overall porosity of the membranes was calculated via the gravimetric method, as typically used for electrospun fiber meshes [58–60]. Briefly, all pores of a membrane sample of known weight and dimensions were completely filled with ethanol by soaking the meshes for 2 h. Porosity was then calculated according to Equation (1):

$$\text{Porosity } (\%) = \frac{Ws_{wet} - Ws_{dry}}{\rho_L V_s} \times 100 \quad (1)$$

in which Where Ws_{wet} and Ws_{dry} indicate the weight of the wet and dry membrane samples, respectively, ρ_L is the density of the wetting liquid, and V_s is the sample volume.

Water contact angle (WCA) testing was performed at room temperature by using the FTA 1000 (First Ten Angstroms, U.K.) instrument. A total of 4 μL of deionized water was dropped onto the surface of each sample by way of an automatic liquid drop dosing system. Images of the drops onto the surface were acquired in the 0.033–300 s time range.

1.1.5.2. Mechanical properties. Mechanical properties were carried out by performing tensile tests with an Instron 3365 equipped with the BioPuls Bath (Instron, Norwood, MA, USA) on rectangular-shaped specimens (10 × 90 mm) cut off from the fibrous structures. Tests were performed in air at room temperature with a crosshead speed of 1 mm min^{-1} for 2 mm, and later at 50 mm min^{-1} until fracture occurred.

1.1.5.3. Acousto-mechanical properties. To assess the acoustic performance of the electrospun fiber meshes as a TM surrogate, we employed a 3D finite-element model (FEM) of the human middle ear developed in previous works in COMSOL 6.1 (COMSOL Multiphysics, Burlington, MA, USA) [61]. This model can simulate linear harmonic vibrations in the middle ear upon sound-pressure stimulations of the eardrum. As reported in Fig. 1, the main components of FEM are the tympanic membrane (subject of our study) and the ossicular chain (composed of the three ossicles: malleus, incus, and stapes). According to earlier studies (e.g., [6,62]), the cochlear load on the stapes was simulated with a cochlear impedance measured experimentally. In the model from [61], the Veronda-Westmann constitutive relation was used to describe the TM behavior under large pressures. In this work, we again used linearized material values, such as the Young's modulus, since only small acoustic pressures are used in the simulations. As in [61], the material parameters are assumed to be constant over the eardrum surface, except for the thickness, which is based on experimentally determined TM thicknesses. Moreover, a shell framework was used to model the TM surface, since this allows for changing the thickness in the model more easily, which is needed to find the optimal thickness for the materials investigated in this paper. The parameters of the middle ear model were validated by comparing the average velocity of the stapes with experimental data presented in [63]. Additionally, we include a baseline result of our model, with a reference Young's modulus (E_{ref}) of 40 MPa and a thickness of 50 μm, respectively.

The benchmarks used to compare data were: the umbo vibration in terms of velocity level amplitude (v_z) and phase, calculated as a function

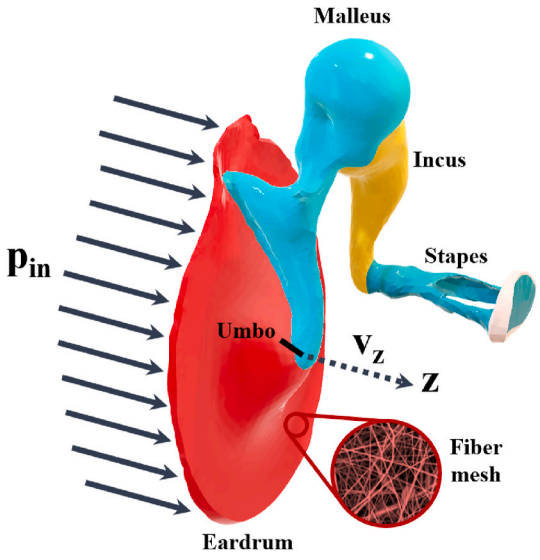

Fig. 1. *In silico* model of the middle ear to test the nanocomposites constituting the eardrum. Note: ligaments and tendons are not shown to keep the figure concise.

of frequency (300–6000 Hz) in response to uniform harmonic sound pressure (p_{in}) on the eardrum of 1 Pa amplitude. Results were also compared to experimental data from [64].

1.2. Statistical analysis

Data collected during the experimental tests were reported using the main statistical descriptors: mean value and standard deviation. When appropriate, a statistical analysis between groups was performed using the Jamovi software (version 2.3.26.0) to assess any significant difference between the datasets. In particular, a Single-Way ANOVA - Post-hoc Tukey Test with a significance level $\alpha = 0.05$ was performed in the analysis.

2. Results and discussion

2.1. Morphological analysis

A comprehensive characterization of electrospun polymeric membranes and their composites GO yielded extensive insights into the effects of GO on the properties of these materials. The morphology of the fiber meshes was investigated using SEM and image analysis techniques. Fig. 2 presents the SEM micrographs of the pure polymeric systems (a-d) and those loaded with graphene oxide GO (a^i-d^i). While neat polymers PCL, PLA, and PLGA exhibited a smooth and homogeneous fibrous structure, the incorporation of GO led to a notable increase in surface roughness, significantly altering the fiber diameter, especially evident in PLA and PLGA fibers.

Furthermore, as observed in Fig. 2 d^i, the addition of GO into PVDF constructs promoted the formation of bubble-like deformations to a greater extent than in the other samples, thus resulting in increased fiber junctions. This is likely due to its well-known tendency to hinder solvent evaporation [30]. It is noteworthy that GO can exhibit a broad distribution of lateral sizes (in the order of tens of micrometers) [65]: in PLA and PLGA systems, GO appeared in an aggregated form on the surface. It was found that larger GO sheets protrude from the fibrous network (Fig. 2 a^i-d^i), with a configuration resembling protrusion with fiber bulging near their presence. This suggests a distinct interaction between the polymeric matrices and GO, likely facilitated by the functional groups in the polymers that interact with GO, in contrast to the less pronounced presence of GO observed in PCL/GO fibers.

The analysis of the diameter distributions of electrospun polymer fibers with and without the addition of GO was conducted using frequency histograms (%) to offer a comprehensive understanding of the modifications induced by the addition of GO (Fig. 3).

Specifically, most of the neat polymeric fiber meshes (Fig. 3a–c) displayed fibers with smooth surface and a discrete diameter distribution, with about 88 % fibers exhibiting submicrometric size diameters ranging in 1–0.2 μm while the remaining were thicker than ~1.4 μm (Fig. 3a–c). In contrast, the PVDF-HFP scaffold (Fig. 3 d) showed pronounced bubble-like phenomena with 34 % of fibers exhibiting submicrometric sizes: 52 % of them presented diameters ranging in 1.4–1.8 μm, while 16 % of them were thicker than 1.8 μm (Fig. 3 d).

The introduction of GO across all utilized polymeric composites significantly influenced the morphology of the electrospun membranes, as depicted in Fig. 3 a^i-d^i. In detail, the histograms reveal that PCL/GO fibers exhibited a higher frequency of larger diameters compared to neat PCL, displaying a higher median and a wider interquartile range (IQR) for PCL/GO (data not shown). This suggests that the addition of GO encourages the formation of fibers with larger and less uniform diameters than their neat counterparts. Similarly, the histograms related to PLA/GO shows a broader distribution than that of the neat PLA. As for the PLGA, the histogram highlights a much narrower diameter distribution with the addition of GO, indicating more significant heterogeneity in fiber size. Furthermore, as observed in Fig. 2 c^i, the fibers are characterized by the GO on the surface (yellow arrows), presumably due to an aggregation effect during the electrospinning process, leading to a substantial morphological change with smaller diameters. The reduction in the average fiber diameter is reflected in an IQR, which is smaller compared to that of pure PLGA and compared to the PLA and PCL, thus suggesting less variability and more precise control over fiber production. In the case of PVDF-HFP, the histogram shows that the introduction of GO alters the fiber diameter distribution but still produces a slight tendency towards smaller diameters, as evidenced by the reduced median in the box plot for the PVDF-HFP/GO. This observation is particularly interesting because it suggests that PVDF-HFP may interact with

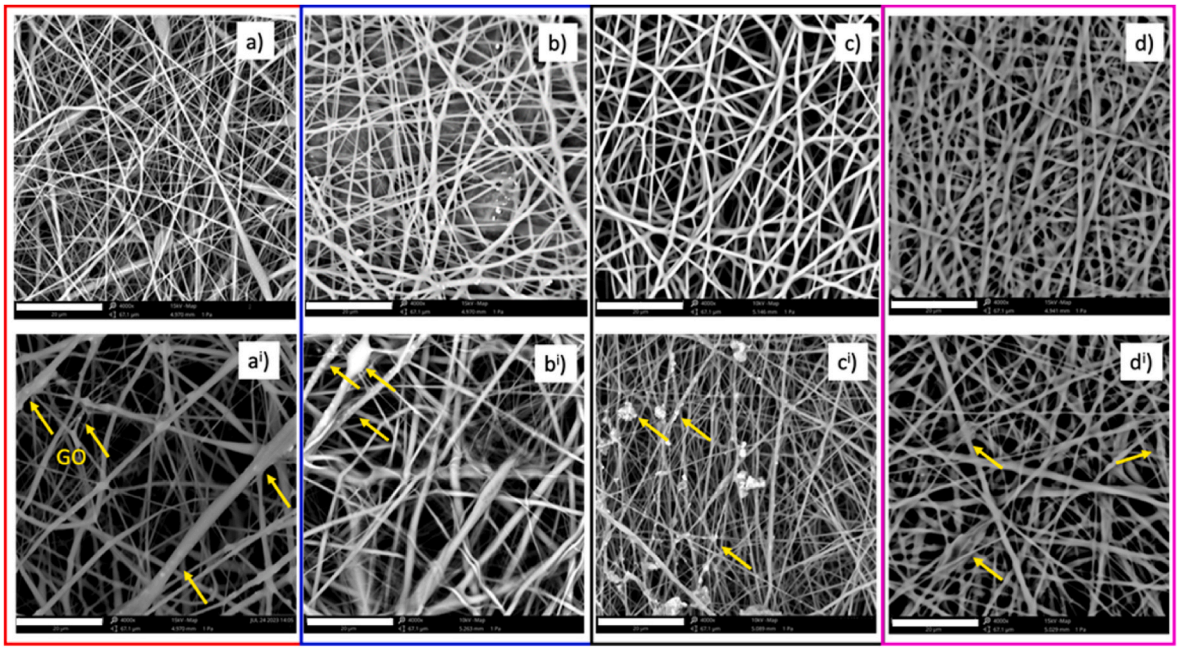

Fig. 2. Morphological analysis of the electrospun membranes. Neat polymers PCL, PLA, PLGA and PVDF-HFP (a–d). Nanocomposites made of a polymer loaded with GO: PCL/GO, PLA/GO, PLGA/GO and PVDF/GO (a^i-d^i). Scale bar is 20 μm.

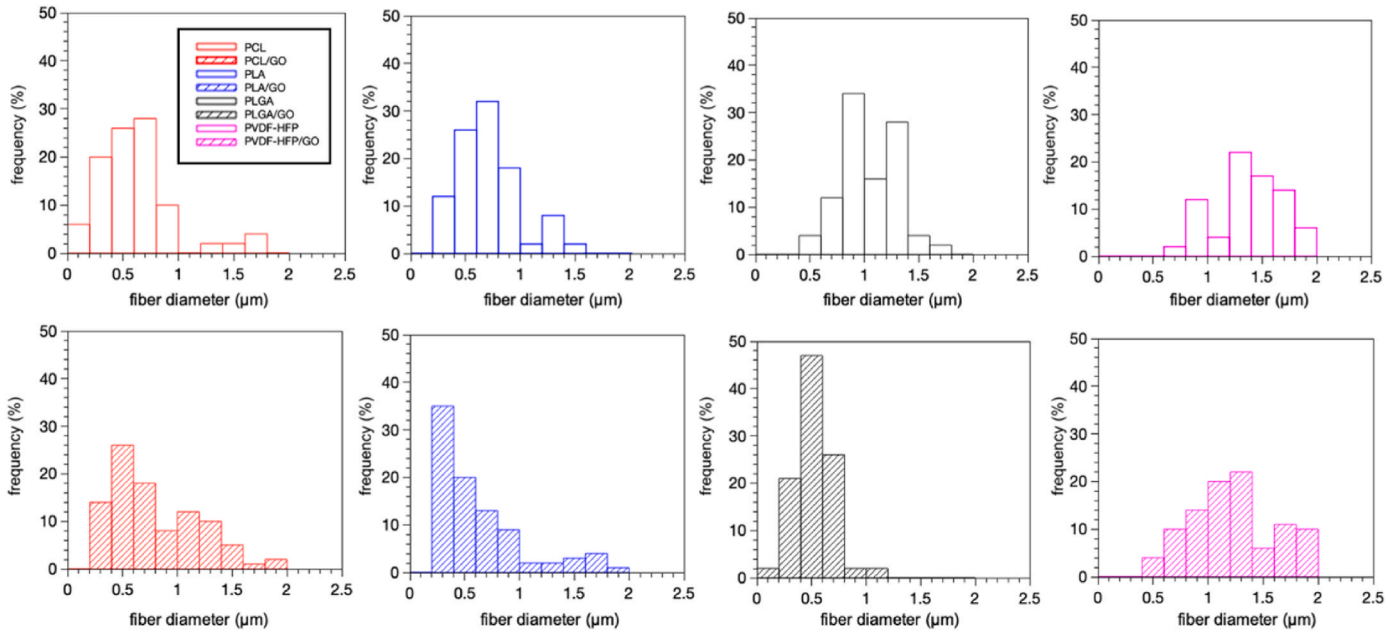

Fig. 3. Distribution of fiber diameters. Histograms depicting the dimension ranges of the fiber diameters. (a, b, c, d) Neat polymers – PCL, PLA, PLGA and PVDF-HFP. (a^i, b^i, c^i, d^i) Polymer/GO nanocomposites.

the GO to minimize the impact on fiber diameter variability. Additionally, as observed in Fig. 1, both the PVDF-HFP membrane and the PVDF-HFP/GO membrane exhibit an interconnected structure characterized by welded fibers and defects, attributable to poor solvent evaporation. The presence of larger diameter fibers for the components loaded with GO, compared to the pure components, can be attributed to the high charge density of the systems, which is known to promote jet splitting, thereby forming fibers that are both thicker and thinner [29,30], with the presence of GO embedded within the fibers. The assessment of the morphologies of the neat polymeric and nanocomposite structures leads to the conclusion that GO alters the physical properties of electrospun fibers in a polymer-dependent manner. These morphological alterations are reflected in the bulk physical properties of the membranes as changes in porosity and density. In particular, referring to Table 2, the nanocomposite fiber meshes revealed a slight decrease in porosity compared to that of neat polymeric counterparts, correlated with an increased density. These modifications suggest the effective incorporation of GO within the polymer matrix, potentially leading to denser fiber packing or the filling of pores between fibers.

2.2. Wettability

WCA measurements, shown in Fig. 4, provides a comprehensive insight into the influence of GO on the hydrophobicity and hydrophilicity of polymer structures, revealing the intricate relationship between microscopic modifications and their interaction with the environment over time. At the beginning of the experiments, we observed high values of WCA, higher than 100°, for all samples with the only exception of PLA/GO and PVDF-HFP/GO. This indicates a hydrophobic behavior of the structures, which slightly decreases over time. This shift is particularly pronounced in PVDF-HFP/GO and PLA/GO samples, which exhibited a specific time-driven transition towards a hydrophilic behavior. PVDF/GO fiber meshes show a WCA that remains stable until 100 s before sharply falling to around 75° after 200 s, hinting at a threshold effect in water-structure surface interaction. The hydrophilic nature of GO, along with its uniform distribution on the fiber surface, is credited for enhancing the wettability of the samples [26,66]. Such changes, confirmed by SEM imagery and quantitative WCA data, suggest that the integration of GO into polymer matrices profoundly alters their microstructural and surface properties. These modifications led to a slight decrease in porosity and an increase in density, indicating enhanced structural characteristics and altered surface wettability. These factors are crucial for a wide range of applications, from biomedicine to environmental engineering, where tailored functionalities are required [67]. SEM images provided a visual proof of the impact of GO on the electrospun fibers, which supports the quantitative findings from WCA measurements. This cohesive understanding underscores the role of GO as a versatile modifier, capable of adjusting structural characteristics to meet specific application needs. The overall decrease in WCA for GO composites underlines the potential of finely balance hydrophobicity and hydrophilicity through GO content manipulation, thus enhancing the potential of these structures in advanced material applications where moisture interaction is essential, such as in filtration, tissue engineering scaffolds, and moisture management materials [44,68,69].

Table 2
Characterization of fibrous architecture of the electrospun structures.

Sample	Porosity [%]	Density [g/cm^3]	Mean fiber diameter (μm)
PCL	90	1.15	0.45
PCL/GO	90	1.16	0.68
PLA	91	1.26	0.7
PLA/GO	88	1.28	0.55
PLGA	87	1.34	1.2
PLGA/GO	86	1.36	0.53
PVDF	84	1.78	1.5
PVDF-HFP/GO	88	1.80	1.4

2.3. Mechanical properties

We evaluated the mechanical properties of the fiber meshes through standard tensile tests, from which the Young's Modulus (E), elongation at break (ε_b), and ultimate stress (UTS) were calculated.

Concerning the Young's modulus, we noticed a statistically significant increment with the introduction of the GO in the polymeric matrix. Such a difference is more marked for the PLGA polymer, as it showed an increase of about 50 MPa. The slightest statistical difference regards, in contrast, the PVDF-HFP (from 0.2 to 0.6 MPa). As for the elongation at

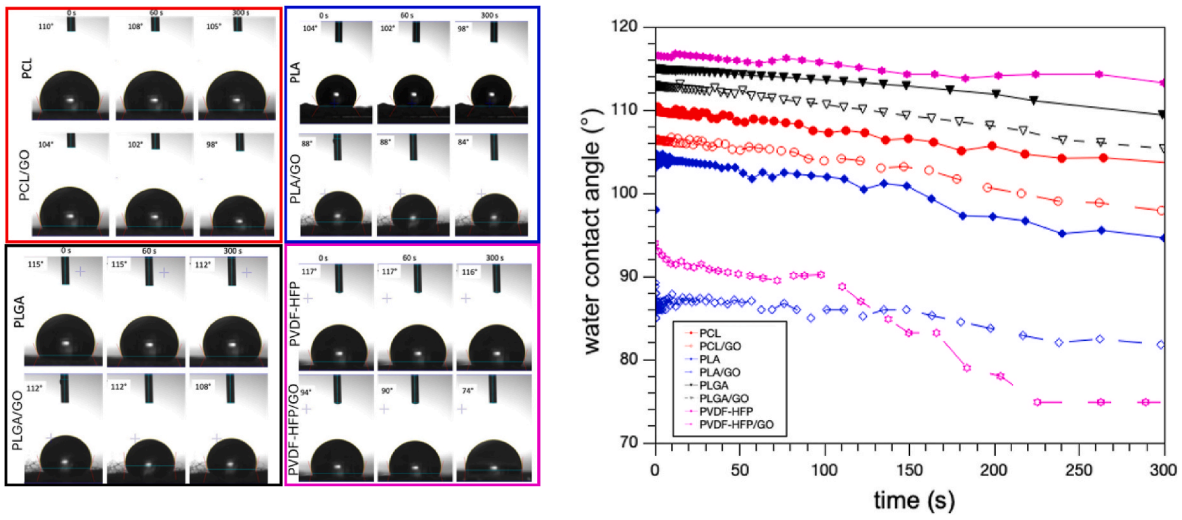

Fig. 4. Water contact angles (WCAs) observed and measured as a function of time on the membranes. (A) Visual assessment of the WCA. (B) Quantitative measurement of the WCA as a function of time.

break, we observed a general reduction in the numerical values in the samples with the introduction of the GO that, however, was not statistically significant for the PLA and PCL samples. The only exception is for the PVDF-HFP, to which the addition of GO increased the ductility (from 90 % to 160 %). The ultimate stress presented the same trend observed for Young's modulus, with statistically relevant differences between the groups. The most marked increments were observed for the PCL and PLGA, for which the UTS almost doubled, from 2.9 to 5.8 MPa and 2.7–4.9 MPa, respectively. Table 3 summarizes the results as mean value ± standard deviation. We also report in Fig. S1, a graphical representation of the results in the form of box plots, where the statistically relevant results between the groups were highlighted.

2.4. *In silico acoustic assessment*

The results of the *in silico* acoustic assessment, reported in Fig. 5A and B, highlight the differences between the curves of the native tissue [64] and our simulations. Fig. 5A reports the umbo velocity amplitude and phase. Mean experimental umbo data is shown as a solid black curve, with the corresponding standard deviation denoted by the shaded area in grey. The solid red curve denotes the results from a baseline model, while all other curves illustrate manufactured TM tissue.

All materials, except for PVDF-HFP, presented curves that are reasonably within the standard deviation of the experimental results. PCL/GO exceeds the standard deviation around 800 Hz, but the difference with the mean experimental curve is only 4 dB, which is within the tolerances used to compare experimental data. Around 1100 Hz, PCL/GO has a sharp anti-resonance and is -9 dB lower in amplitude than the mean experimental curve. However, the bandwidth of this drop is small, so the effect of the overall response of PCL/GO from a physiological standpoint will be negligible. PCL- and PLGA-based membranes (dotted lines) did not present significant changes in their behavior with the addition of GO (solid lines) for both the amplitude and the phase.

For PVDF-HFP, adding GO shifted the resonance towards the higher frequencies. It has to be noticed that the response of PVDF-HFP is very erratic, which resulted unsuitable to conduct sound over the normal hearing range. For PLA, the effect of adding GO was also pronounced. Moreover, the PLA/GO curve tracked the baseline model closely.

Table 4 illustrates the vibration patterns of the native TM, and a selection of its substitutes at frequencies of 250 Hz, 1000 Hz, and 4000 Hz. The color scale represents the out-of-plane motion "w", i.e., in the direction towards or away from the ossicles. As reported in previous studies, the TM vibrates to transfer acoustic sounds to the ossicles of the middle ear while dissipating, at its best, any potential harmful energy input (i.e., loud sounds) [70]. The motion of the native TM is location-/frequency-dependent, based on the structural conformation of the eardrum, composed of oriented collagen fibers, and the connections with the surrounding tissues, namely a fixed attachment on its periphery and, approximately in its middle, with the malleus (Table 4 – row Native TM) [5]. We report, as relevant showcases, the results obtained for the TM substitutes based on PLGA and PVDF-HFP. The PLGA-based TM substitutes, independently of the presence of the GO, show little vibration differences at 250 Hz and 1000 Hz with respect to the native TM, in the order of 10 dB, equal to a few nanometers. At 4000 Hz, the high frequency modes of the native TM and PLGA-based structures are different in shape but, however, of the same order of magnitude, thus resulting in a similar behavior.

In contrast, the PVDF-HFP substitutes possess a lower stiffness, and therefore a lower resonant frequency, which leads at 250 Hz to significant higher vibrations far from the malleus, whose motion remains similar to that observed for the native TM. At 1000 Hz, the vibrations tend to be slightly closer to the native TM, but present large variations across the surface. Finally, at 4000 Hz, high vibration orders are visible across the surface with amplitudes significantly lower (more than 20 dB) than that those of the native TM. The addition of GO has a flattening effect of about 20 dB, which results beneficial at frequencies up to 1000 Hz, making the TM vibration modes closer – but still different – to the native TM, but highly negative at higher frequencies (4000 Hz), since the discrepancies already observed without GO are emphasized.

A step towards an optimization of the outcomes consisted of tuning the thickness of the membranes to improve the general performance of the device. While the results for PCL- and PLA-based materials did not present significant differences, PLGA- and PVDF-HFP-based materials presented a slight improvement. Referring to Fig. 6, we observed that, reducing the thicknesses down to 30 μm, both materials led to a shift of

Table 3
Summary of the mechanical properties of the fiber structures.

Base material	Filler	E [MPa]	ε_b [%]	UTS [MPa]
PLA	–	37.7 ± 7.9	220 ± 30	3.2 ± 0.2
	GO	53.0 ± 11.3	210 ± 30	4.0 ± 0.1
PCL	–	5.3 ± 0.8	130 ± 10	2.9 ± 0.4
	GO	18.5 ± 2.1	110 ± 10	5.8 ± 0.8
PLGA	–	118.0 ± 6.0	110 ± 10	2.7 ± 0.2
	GO	189.0 ± 14.7	90 ± 10	4.9 ± 0.4
PVDF	–	0.2 ± 0.01	90 ± 10	1.0 ± 0.1
	GO	0.6 ± 0.04	160 ± 20	1.2 ± 0.3

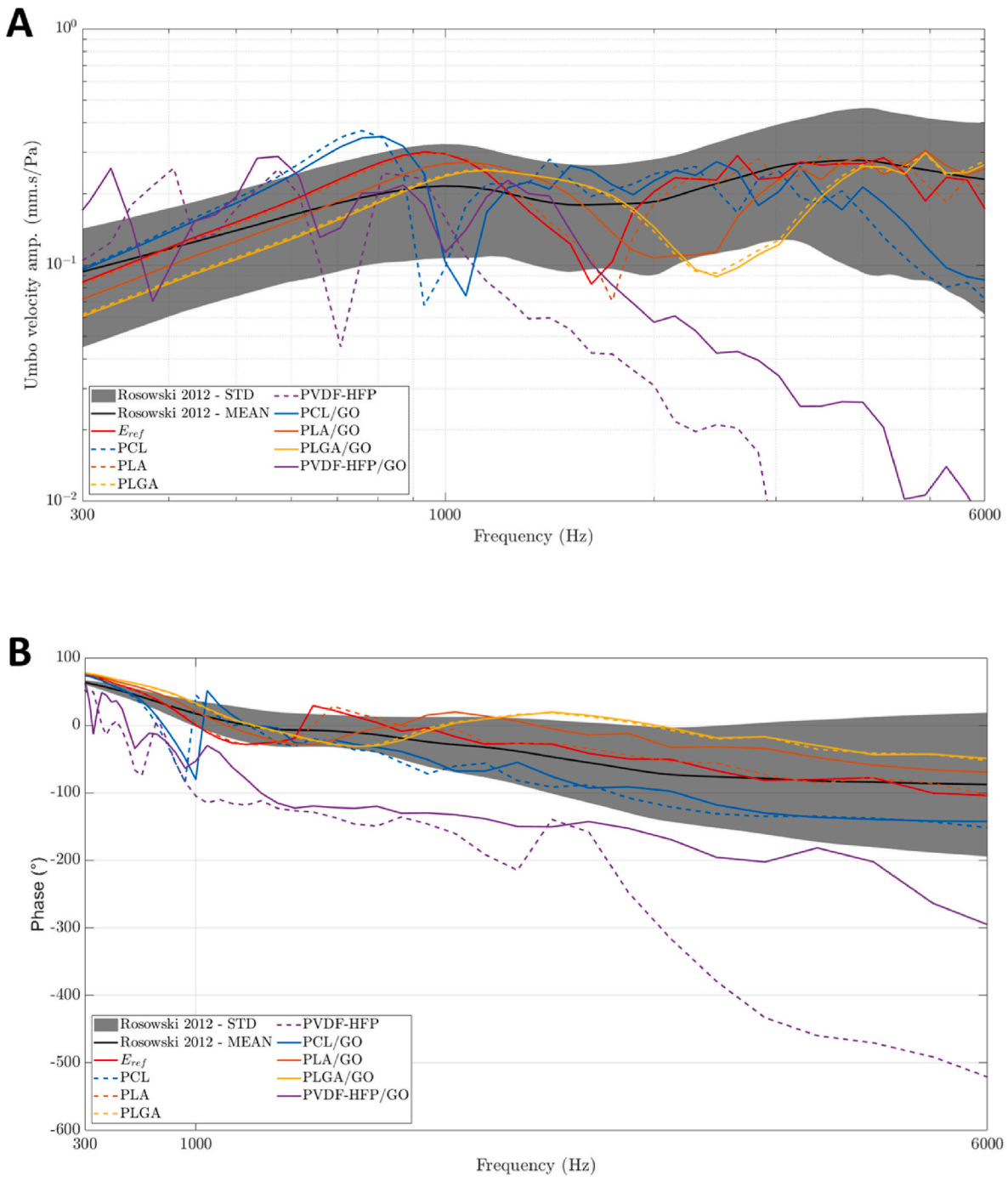

Fig. 5. Acousto-mechanic characterization of the developed membranes and comparison with results from a validated *in silico* model (red line) and experimental measurements (black line – average value and shaded area – standard deviation) from Ref. [64]. Umbo velocity amplitude (A) and phase (B). Note that the PVDF-HFP-based membranes cannot mimic the native tissue properly. As shown in the Supplementary Material, a simple variation of the thickness is not sufficient to match the desired outcome. (For interpretation of the references to color in this figure legend, the reader is referred to the Web version of this article.)

the resonant peak to 1 kHz, one of the critical frequencies. However, the PVDF-HFP-based samples did not improve their performance significantly at frequencies above 2 kHz.

2.5. Relatabilty with previous studies from literature

Aiming at comparing the results in this manuscript with those from literature, it is possible to state that it is possible to perform a comparative analysis on the intrinsic properties of the materials (of interest for this specific application) in terms of density, stiffness, ultimate stress, and elongation at break, but a direct comparison on the acoustic performance – the most important benchmark – is hard to achieve. This is because there are three different approaches to recover the TM based on the clinical needs: i) fabrication of patches; ii) design and fabrication of bioinspired structures; iii) development of biomimetic structures. In the first case, the tympanic membrane is partially present, and the patches are used to fill the gaps that the tissue is not able to recover passively. In the second case, the shape of the replacement does not follow the morphology of the native TM but, in contrast, simplified geometries (e.g., flat surfaces) are designed to behave similarly to the native tissue.

Table 4
Graphical representation of the vibration of TM substitutes against that of the native TM across benchmark frequencies. The scale bar denotes the out-of-plane motion w for the native TM (first row). For all other curves (second row onwards), the change in w with respect to the native TM is given in a decibels (dB) scale to better visualize the differences in the vibration patterns. Note: 0 dB corresponds to 1 nm while 40 dB is equal to 100 nm.

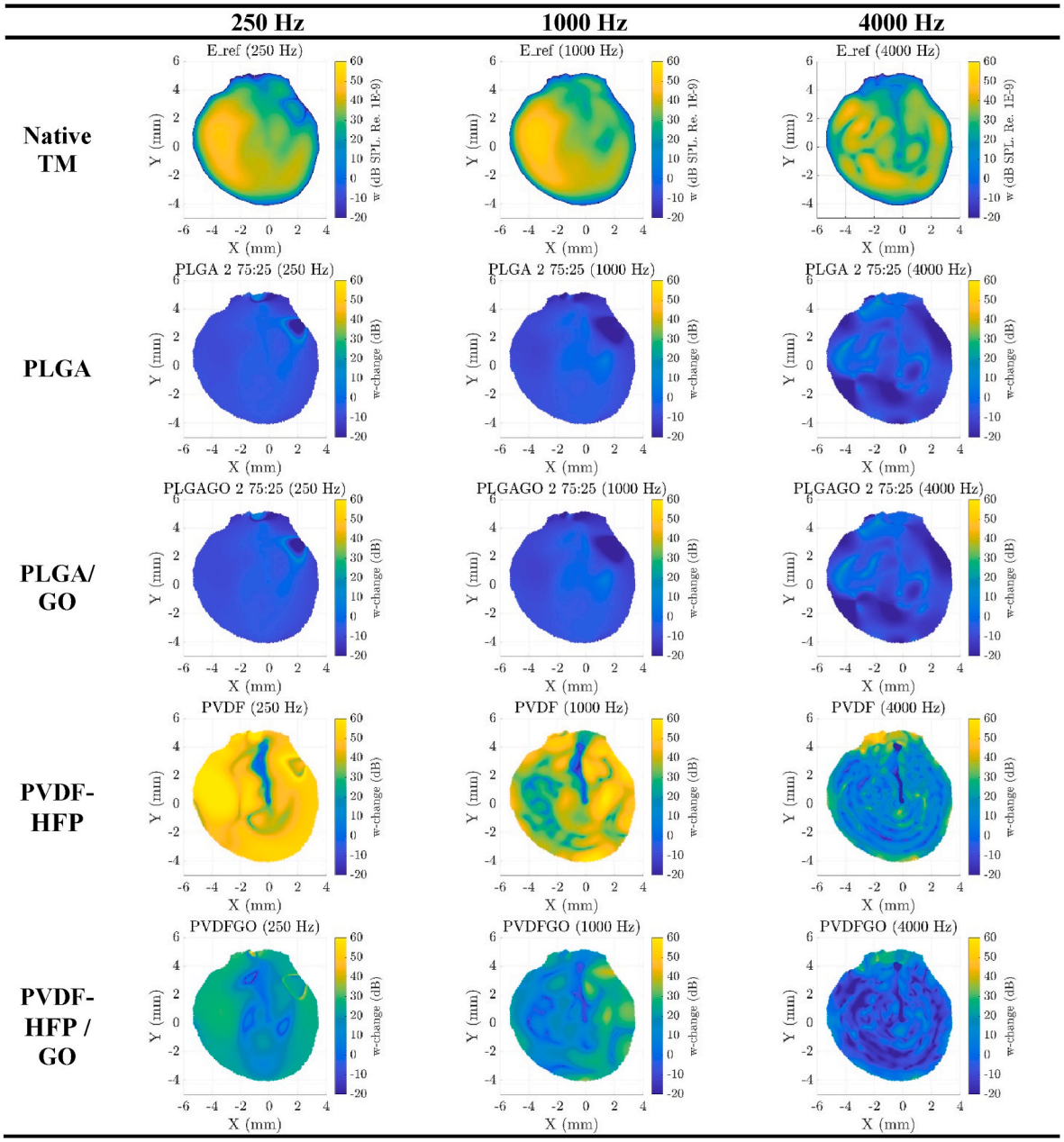

The third case, aims at recreating the exact geometry and functionalities of the native tissue [9].

Our approach lies between cases ii) and iii) since we aim at developing a structure with the same morphology but without the structural complexity possessed by the native TM. After considering this premise, aiming at providing an overall comparison, we provide some data from literature.

Kuru et al. developed a bench model of the middle ear using silicon rubber to cast the soft tissues (including the TM). Based on the hardness of the materials, they created different models of the middle ear with acoustic behaviors that fell within the ranges expressed by Rosowski in his experimental tests. This model, however, is a mock-up of the actual ear and, although promising, the results obtained with the silicon rubber have not been confirmed *ex* or *in vivo* [71].

Kozin et al. developed a flat spider web-like structure via 3D printing using different materials like Polydimethylsiloxane (PDMS), PCL, and PLA. The acoustic behavior was assessed by measuring the velocity at the center of the grafts (the position that should be closed to the actual umbo) with a laser doppler vibrometer (LDV), and compared the outcomes with those of the temporalis fascia and the actual umbo in a normal ear. The results showed that all the materials, including the temporalis fascia behaved even better that the normal ear with velocity amplitudes generally higher than that of the umbo in a normal ear. However, these results have not been confirmed in an *ex vivo* or *in vivo* model where these devices should be actually connected to the ossicular chain [72].

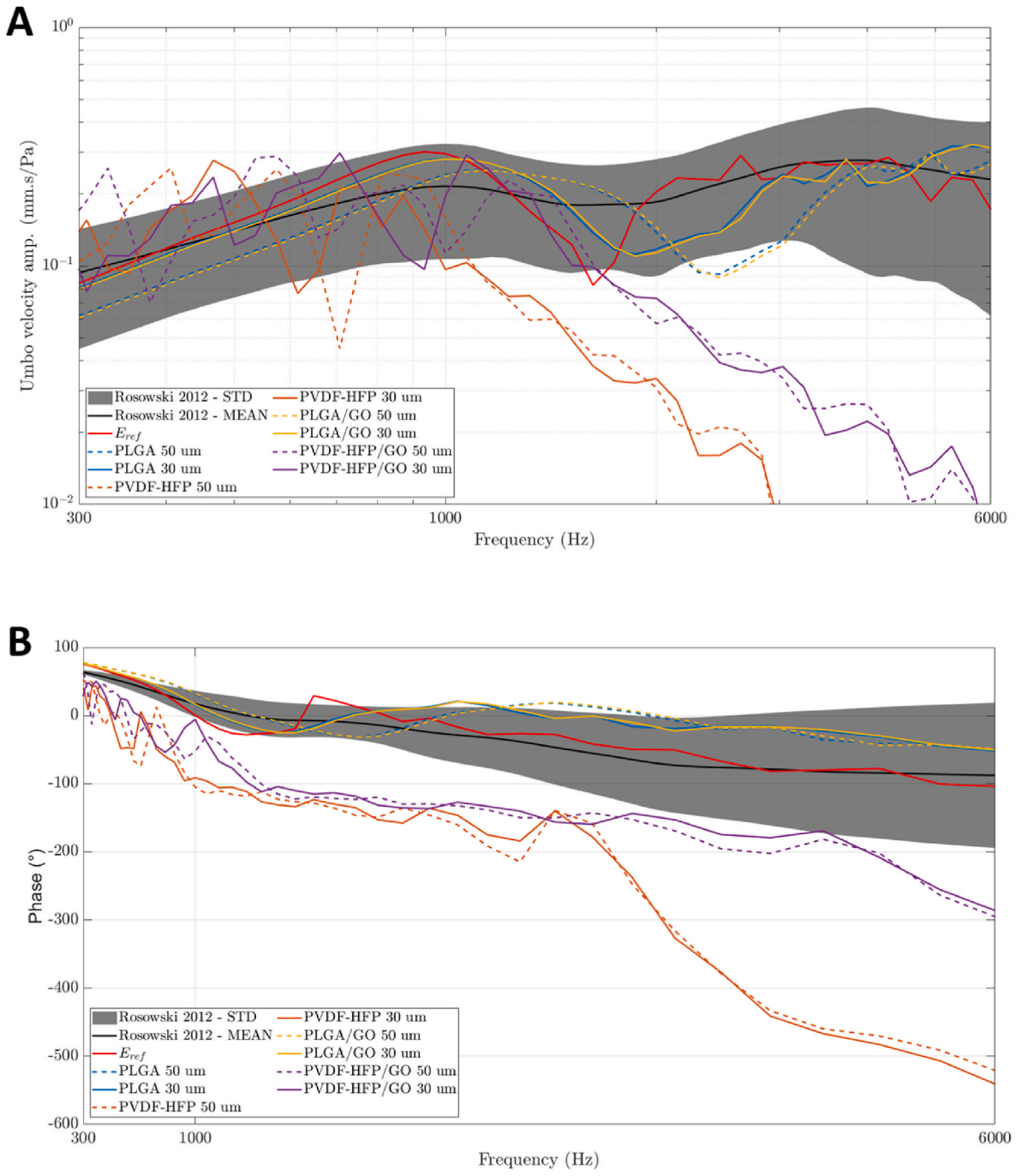

Fig. 6. Acousto-mechanic characterization of the developed membranes and comparison with results from a validated in-silico model (red line) and experimental measurements (black line – average value and shaded area – standard deviation) from Ref. [59]. Results using membranes with thicknesses reduced to 30 μm. Umbo velocity amplitude (A) and phase (B). All other samples showed negligible differences in the results (data not shown). (For interpretation of the references to color in this figure legend, the reader is referred to the Web version of this article.)

Anand et al. presented a study in which they showed the significance of the geometry (presence/absence of rigid features) of a TM replacement on its biological and acoustic properties. All samples were made of 300 PEOT55PBT45, a grade of PEOT/PBT copolymer, and fabricated through a synergistic approach involving electrospinning and 3D printing. To assess the acoustic behavior, they used the LDV to measure the velocity at the center of the specimens, and compared the results with the outcomes from a native tissue. The results showed that the velocities measured on all the specimens were higher than that of the normal ear up to about 1 kHz. However, the cases in which the samples presents more complex features (e.g., rigid radial fibers), showed a suboptimal behavior after 1 kHz thus highlighting the need for a redesign of the devices for high frequencies [40]. Therefore, it is difficult to make a comparison of these results with those provided in this work because of the different employed design approaches and ways of assessment.

3. Conclusions

The development of functionalized nanocomposites is one of the most intriguing topics in Materials Science and Engineering. In this work, we present the development of electrospun polymeric

nanocomposite fiber meshes embedding GO nanosheets for acoustic applications, namely, to be used as eardrum replacement material. We assessed the influence of GO on the physico-chemical and acousto-mechanical properties of the electrospun membranes by combining experimental and computational techniques.

The experimental work resulted in a comprehensive characterization of the different materials investigated. As expected, the effect of adding GO increased the stiffness of the resulting fiber membranes.

Using these experimental results, we investigated the acoustic behavior of the nanocomposites by exploiting a FEM of the middle ear, in which the material properties of the eardrum were altered to match the composites of this study. Except for PVDF-HFP, the effect of adding GO to the materials studied (i.e., in PCL, PLA, PLGA) was rather small for the eventual stapes velocity response. Of note is that PLA/GO tracked the baseline model, therefore mimicking a typical human eardrum, the best, making it the most suitable eardrum graft material according to the data presented in this paper.

Our approach, although applied to a specific biomedical application, paves the way to the development of acoustically-functionalized electrospun meshes with uses not limited to the bioengineering field.

Funding declaration

This study was partially supported by the 4NanoEARDRM project, under the frame of EuroNano-Med III, an ERA-NET Cofund scheme of the Horizon 2020, Research and Innovation Framework Program of the European Commission, via the Italian Ministry of Education, University and Research (MIUR, grant number B56H18000140001). M.M. and S.D. acknowledge the Plan for National Recovery and Resilience (PNRR, Mission 4 Component 2 Investment 1.4 - Italian Ministry of University and Research funded by the European Union – NextGenerationEU), Project "HPC, Big Data and Quantum Computing (CN1)", Spoke 7 (code CN00000013, CUP I53C22000690001).

CRediT authorship contribution statement

Mario Milazzo: Writing – review & editing, Writing – original draft, Visualization, Validation, Supervision, Software, Resources, Project administration, Methodology, Investigation, Funding acquisition, Formal analysis, Data curation, Conceptualization. **Serena Danti:** Writing – review & editing, Writing – original draft, Visualization, Validation, Investigation, Funding acquisition, Formal analysis, Data curation. **Pieter Livens:** Writing – review & editing, Writing – original draft, Visualization, Validation, Software, Methodology, Investigation, Formal analysis, Data curation, Conceptualization. **Joris Dirckx:** Writing – review & editing, Writing – original draft, Visualization, Validation, Supervision, Software, Methodology, Investigation, Funding acquisition, Formal analysis, Data curation. **Roberto Scaffaro:** Writing – review & editing, Writing – original draft, Visualization, Validation, Supervision, Software, Resources, Project administration, Methodology, Investigation, Funding acquisition, Formal analysis, Data curation, Conceptualization. **Michele Gammino:** Writing – review & editing, Writing – original draft, Visualization, Validation, Methodology, Investigation, Formal analysis, Data curation, Conceptualization.

Declaration of competing interest

The authors declare that they have no known competing financial interests or personal relationships that could have appeared to influence the work reported in this paper.

Data availability

Data will be made available on request.

Appendix A. Supplementary data

Supplementary data to this article can be found online at https://doi.org/10.1016/j.coco.2024.102048.

References

[1] D.R. Raichel, The Science and Applications of Acoustics, 2003.
[2] World Health Organization, Deafness and hearing loss. https://www.who.int/news-room/fact-sheets/detail/deafness-and-hearing-loss, 2024.
[3] G. Volandri, F. Di Puccio, P. Forte, C. Carmignani, Biomechanics of the tympanic membrane, J. Biomech. (2011), https://doi.org/10.1016/j.jbiomech.2010.12.023.
[4] O. Nobus, L. Parmentier, P. Livens, P. Muyshondt, K. Szewcyk, C. Jacobs, D. Verdoodt, L. Pieters, Q. Thijssen, B. Van Durme, others, The importance of mechanical and biological cues of tympanic membrane grafts to ensure optimal regeneration, Biomater. Adv. (2024) 213827.
[5] M. Milazzo, E. Fallah, M. Carapezza, N.S. Kumar, J.H. Lei, E.S. Olson, The path of a click stimulus from ear canal to umbo, Hear. Res. 346 (2017) 1–13.
[6] M. Milazzo, P.G.G. Muyshondt, J. Carstensen, J.J.J. Dirckx, S. Danti, M.J. Buehler, De novo topology optimization of total ossicular replacement prostheses, J. Mech. Behav. Biomed. Mater. 103 (2020) 103541.
[7] S. Danti, D. D'Alessandro, A. Pietrabissa, M. Petrini, S. Berrettini, Development of tissue-engineered substitutes of the ear ossicles: PORP-shaped poly(propylene fumarate)-based scaffolds cultured with human mesenchymal stromal cells, J. Biomed. Mater. Res., Part A A (2010), https://doi.org/10.1002/jbm.a.32447.
[8] M. Milazzo, S. Danti, F. Inglese, G. van Vuuren, V. Gramigna, G. Bonsignori, A. De Vito, L. Bruschini, C. Stefanini, S. Berrettini, Ossicular replacement prostheses from banked bone with ergonomic and functional geometry, J. Biomed. Mater. Res. Part B Appl. Biomater. 105 (2017) 2495–2506.
[9] S. Anand, S. Danti, L. Moroni, C. Mota, Regenerative therapies for tympanic membrane, Prog. Mater. Sci. (2022) 100942.
[10] J.H. Kim, J.-H. Bae, K.T. Lim, P.-H. Choung, J.-S. Park, S.J. Choi, A.L. Im, E.T. Lee, Y.-H. Choung, J.H. Chung, Development of water-insoluble chitosan patch scaffold to repair traumatic tympanic membrane perforations, J. Biomed. Mater. Res., Part A 90A (2009) 446–455, https://doi.org/10.1002/jbm.a.32119.
[11] A.A. Aarnisalo, J.T. Cheng, M.E. Ravicz, N. Hulli, E.J. Harrington, M.S. Hernandez-Montes, C. Furlong, S.N. Merchant, J.J. Rosowski, Middle ear mechanics of cartilage tympanoplasty evaluated by laser holography and vibrometry, Otol. Neurotol. 30 (2009) 1209–1214.
[12] M. Makuszewska, M. Sokołowska, E. Hassmann-Poznańska, I. Bialuk, B. Skotnicka, T. Bonda, J. Reszeć, M.M. Winnicka, Enhanced expression of hepatocyte growth factor in the healing of experimental acute tympanic membrane perforation, Int. J. Pediatr. Otorhinolaryngol. 79 (2015) 987–992.
[13] J.R.M. Aerts, J.J.J. Dirckx, Nonlinearity in eardrum vibration as a function of frequency and sound pressure, Hear. Res. 263 (2010) 26–32.
[14] B. Levin, R. Rajkhowa, S.L. Redmond, M.D. Atlas, Grafts in myringoplasty: utilizing a silk fibroin scaffold as a novel device, Expet Rev. Med. Dev. 6 (2009) 653–664.
[15] P. Hong, M. Bance, P.F. Gratzer, Repair of tympanic membrane perforation using novel adjuvant therapies: a contemporary review of experimental and tissue engineering studies, Int. J. Pediatr. Otorhinolaryngol. 77 (2013) 3–12.
[16] X. Yan, M. Yu, S. Ramakrishna, S.J. Russell, Y.-Z. Long, Advances in portable electrospinning devices for in situ delivery of personalized wound care, Nanoscale 11 (2019) 19166–19178.
[17] W. Shao, J. He, F. Sang, B. Ding, L. Chen, S. Cui, K. Li, Q. Han, W. Tan, Coaxial electrospun aligned tussah silk fibroin nanostructured fiber scaffolds embedded with hydroxyapatite–tussah silk fibroin nanoparticles for bone tissue engineering, Mater. Sci. Eng. C 58 (2016) 342–351.
[18] B.M. Teh, R.J. Marano, Y. Shen, P.L. Friedland, R.J. Dilley, M.D. Atlas, Tissue engineering of the tympanic membrane, Tissue Eng., Part B 19 (2013) 116–132.
[19] J.H. Kim, S.J. Choi, J.-S. Park, K.T. Lim, P.-H. Choung, S.W. Kim, J. Bin Lee, J. H. Chung, Y.-H. Choung, Tympanic membrane regeneration using a water-soluble chitosan patch, Tissue Eng. 16 (2010) 225–232.
[20] N. Majumder, S. Seit, N.S. Bhabesh, S. Ghosh, An advanced bioconjugation strategy for covalent tethering of TGF$β$3 with silk fibroin matrices and its implications in the chondrogenesis profile of human BMSCs and human chondrocytes: a paradigm shift in cartilage tissue engineering, Adv. Healthcare Mater. (2024) 2303513.
[21] D. Schwarz, D. Pazen, K. Gosz, S. Schwarz, M. Nünning, A.-O. Gostian, L. Koerber, R. Breiter, N. Rotter, D. Beutner, Acoustic properties of collagenous matrices of xenogenic origin for tympanic membrane reconstruction, Otol. Neurotol. 37 (2016) 692–697.
[22] R. Scaffaro, A. Maio, M. Gammino, F.P. La Mantia, Effect of an organoclay on the photochemical transformations of a PBAT/PLA blend and morpho-chemical features of crosslinked networks, Polym. Degrad. Stabil. 187 (2021) 109549.
[23] R. Scaffaro, A. Maio, M. Gammino, Hybrid biocomposites based on polylactic acid and natural fillers from Chamaerops humilis dwarf palm and Posidonia oceanica leaves, Adv. Compos. Hybrid Mater. 5 (2022) 1988–2001.
[24] E. Capuana, F. Lopresti, M. Ceraulo, V. La Carrubba, Poly-L-lactic acid (PLLA)-based biomaterials for regenerative medicine: a review on processing and applications, Polymers 14 (2022) 1153.
[25] M. Milazzo, N. Contessi Negrini, S. Scialla, B. Marelli, S. Farè, S. Danti, M. J. Buehler, Additive manufacturing approaches for hydroxyapatite-reinforced composites, Adv. Funct. Mater. 29 (2019) 1903055, https://doi.org/10.1002/adfm.201903055.

[26] R. Scaffaro, M. Gammino, A. Maio, Wet electrospinning-aided self-assembly of multifunctional GO-CNT@ PCL core-shell nanocomposites with spider leg bioinspired hierarchical architectures, Compos. Sci. Technol. 221 (2022) 109363.
[27] A. Maio, M. Gammino, E.F. Gulino, B. Megna, P. Fara, R. Scaffaro, Rapid one-step fabrication of graphene oxide-decorated polycaprolactone three-dimensional templates for water treatment, ACS Appl. Polym. Mater. 2 (2020) 4993–5005.
[28] H. Lee, C.H. Jang, G.H. Kim, A polycaprolactone/silk-fibroin nanofibrous composite combined with human umbilical cord serum for subacute tympanic membrane perforation; an in vitro and in vivo study, J. Mater. Chem. B 2 (2014) 2703–2713.
[29] R. Scaffaro, A. Maio, M. Gammino, Electrospun polymeric nanohybrids with outstanding pollutants adsorption and electroactivity for water treatment and sensing devices, Adv. Compos. Hybrid Mater. 7 (2024) 13.
[30] R. Scaffaro, M. Gammino, A. Maio, Hierarchically structured hybrid membranes for continuous wastewater treatment via the integration of adsorption and membrane ultrafiltration mechanisms, Polymers 15 (2022) 156.
[31] A. Das, T. Ringu, S. Ghosh, N. Pramanik, A comprehensive review on recent advances in preparation, physicochemical characterization, and bioengineering applications of biopolymers, Polym. Bull. 80 (2023) 7247–7312.
[32] G.G. Flores-Rojas, B. Gómez-Lazaro, F. López-Saucedo, R. Vera-Graziano, E. Bucio, E. Mendizábal, Electrospun scaffolds for tissue engineering: a review, Macromolecules (Washington, DC, U. S.) 3 (2023) 524–553.
[33] M. Rahmati, D.K. Mills, A.M. Urbanska, M.R. Saeb, J.R. Venugopal, S. Ramakrishna, M. Mozafari, Electrospinning for tissue engineering applications, Prog. Mater. Sci. 117 (2021) 100721, https://doi.org/10.1016/J.PMATSCI.2020.100721.
[34] B. Azimi, M. Milazzo, A. Lazzeri, S. Berrettini, M.J. Uddin, Z. Qin, M.J. Buehler, S. Danti, Electrospinning piezoelectric fibers for biocompatible devices, Adv. Healthcare Mater. 9 (2020) 1901287.
[35] B. Sarkodie, J. Amesimeku, C. Frimpong, E.K. Howard, Q. Feng, Z. Xu, Photocatalytic degradation of dyes by novel electrospun nanofibers: a review, Chemosphere 313 (2023) 137654.
[36] C. Anushree, F.A. Rahim, S.C. Vanithakumari, C. Thinaharan, J. Philip, Electrospun superparamagnetic fibrous composite nanofiber films for enhanced oil spill recovery: effect of capping and magnetic nanoparticle loading on oil sorption efficiency, Composer Part A Appl. Sci. Manuf. 171 (2023) 107591.
[37] M. Duan, J. Sun, Y. Huang, H. Jiang, Y. Hu, J. Pang, C. Wu, Electrospun gelatin/chitosan nanofibers containing curcumin for multifunctional food packaging, Food Sci. Hum. Wellness 12 (2023) 614–621.
[38] K. Chen, Y. Li, Y. Li, Y. Tan, Y. Liu, W. Pan, G. Tan, Stimuli-responsive electrospun nanofibers for drug delivery, cancer therapy, wound dressing, and tissue engineering, J. Nanobiotechnol. 21 (2023) 237.
[39] C. Mota, S. Danti, D. D'Alessandro, L. Trombi, C. Ricci, D. Puppi, D. Dinucci, M. Milazzo, C. Stefanini, F. Chiellini, L. Moroni, S. Berrettini, Multiscale fabrication of biomimetic scaffolds for tympanic membrane tissue engineering, Biofabrication 7 (2015) 025005, https://doi.org/10.1088/1758-5090/7/2/025005.
[40] S. Anand, T. Stoppe, M. Lucena, T. Rademakers, M. Neudert, S. Danti, L. Moroni, C. Mota, Mimicking the human tympanic membrane: the significance of scaffold geometry, Adv. Healthcare Mater. 2002082 (2021) 1–16, https://doi.org/10.1002/adhm.202002082.
[41] L. Benecke, Z. Chen, I. Zeidler-Rentzsch, M. von Witzleben, M. Bornitz, T. Zahnert, M. Neudert, C. Cherif, D. Aibibu, Development of electrospun, biomimetic tympanic membrane implants with tunable mechanical and oscillatory properties for myringoplasty, Biomater. Sci. 10 (2022) 2287–2301.
[42] P. Majumder, R. Gangopadhyay, Evolution of graphene oxide (GO)-based nanohybrid materials with diverse compositions: an overview, RSC Adv. 12 (2022) 5686–5719.
[43] R. Salerno-Goncalves, A. Fasano, M.B. Sztein, Engineering of a multicellular organotypic model of the human intestinal mucosa, Gastroenterology 141 (2011) e18–e20.
[44] A.D.B.L. Ferreira, P.R.O. Nóvoa, A.T. Marques, Multifunctional material systems: a state-of-the-art review, Compos. Struct. 151 (2016) 3–35.
[45] C. Shuai, B. Peng, P. Feng, L. Yu, R. Lai, A. Min, In situ synthesis of hydroxyapatite nanorods on graphene oxide nanosheets and their reinforcement in biopolymer scaffold, J. Adv. Res. 35 (2022) 13–24.
[46] P. Feng, S. Shen, L. Yang, Y. Kong, S. Yang, C. Shuai, Vertical and uniform growth of MoS2 nanosheets on GO nanosheets for efficient mechanical reinforcement in polymer scaffold, Virtual Phys. Prototyp. 18 (2023) e2115384.
[47] P. Feng, S. Shen, Y. Shuai, S. Peng, C. Shuai, S. Chen, PLLA grafting draws GO from PGA phase to the interface in PLLA/PGA bone scaffold owing enhanced interfacial interaction, Sustain. Mater. Technol. 35 (2023) e00566.
[48] D.C. Marcano, D. V Kosynkin, J.M. Berlin, A. Sinitskii, Z. Sun, A. Slesarev, L. B. Alemany, W. Lu, J.M. Tour, Improved synthesis of graphene oxide, ACS Nano 4 (2010) 4806–4814.
[49] R. Scaffaro, A. Maio, Influence of oxidation level of graphene oxide on the mechanical performance and photo-oxidation resistance of a polyamide 6, Polymers 11 (2019) 857.
[50] A. Maio, R. Scaffaro, L. Lentini, A.P. Piccionello, I. Pibiri, Perfluorocarbons–graphene oxide nanoplatforms as biocompatible oxygen reservoirs, Chem. Eng. J. 334 (2018) 54–65.
[51] A. Maio, D. Giallombardo, R. Scaffaro, A.P. Piccionello, I. Pibiri, Synthesis of a fluorinated graphene oxide–silica nanohybrid: improving oxygen affinity, RSC Adv. 6 (2016) 46037–46047.
[52] A. Maio, S. Agnello, R. Khatibi, L. Botta, A. Alessi, A. Piazza, G. Buscarino, A. Mezzi, G. Pantaleo, R. Scaffaro, A rapid and eco-friendly route to synthesize graphene-doped silica nanohybrids, J. Alloys Compd. 664 (2016) 428–438.
[53] R. Scaffaro, A. Maio, E.F. Gulino, G.D.M. Micale, PLA-based functionally graded laminates for tunable controlled release of carvacrol obtained by combining electrospinning with solvent casting, React. Funct. Polym. 148 (2020) 104490.
[54] R. Scaffaro, F. Lopresti, A. Maio, L. Botta, S. Rigogliuso, G. Ghersi, Electrospun PCL/GO-g-PEG structures: processing-morphology-properties relationships, Composer Part A Appl. Sci. Manuf. 92 (2017) 97–107.
[55] C.A. Schneider, W.S. Rasband, K.W. Eliceiri, NIH Image to ImageJ: 25 years of image analysis, Nat. Methods 9 (2012) 671–675.
[56] N.A. Hotaling, K. Bharti, H. Kriel, C.G. Simon Jr., DiameterJ: a validated open source nanofiber diameter measurement tool, Biomaterials 61 (2015) 327–338.
[57] F.H. She, K.L. Tung, L.X. Kong, Calculation of effective pore diameters in porous filtration membranes with image analysis, Robot. Comput. Integrated Manuf. 24 (2008) 427–434.
[58] F.E. Ahmed, B.S. Lalia, N. Hilal, R. Hashaikeh, Underwater superoleophobic cellulose/electrospun PVDF–HFP membranes for efficient oil/water separation, Desalination 344 (2014) 48–54.
[59] M. Amirilargani, A. Sabetghadam, T. Mohammadi, Polyethersulfone/polyacrylonitrile blend ultrafiltration membranes with different molecular weight of polyethylene glycol: preparation, morphology and antifouling properties, Polym. Adv. Technol. 23 (2012) 398–407.
[60] Y. Liao, R. Wang, M. Tian, C. Qiu, A.G. Fane, Fabrication of polyvinylidene fluoride (PVDF) nanofiber membranes by electro-spinning for direct contact membrane distillation, J. Membr. Sci. 425 (2013) 30–39.
[61] P.G.G. Muyshondt, J.J.J. Dirckx, Structural stiffening in the human middle ear due to static pressure: finite-element analysis of combined static and dynamic middle-ear behavior, Hear. Res. 400 (2021) 108116.
[62] S. Puria, W.T. Peake, J.J. Rosowski, Sound-pressure measurements in the cochlear vestibule of human-cadaver ears, J. Acoust. Soc. Am. (1997), https://doi.org/10.1121/1.418563.
[63] J.J. Rosowski, W. Chien, M.E. Ravicz, S.N. Merchant, Testing a method for quantifying the output of implantable middle ear hearing devices, Audiol. Neurootol. (2007), https://doi.org/10.1159/000101474.
[64] J.J. Rosowski, H.H. Nakajima, M.A. Hamade, L. Mafoud, G.R. Merchant, C. F. Halpin, S.N. Merchant, Ear-canal reflectance, umbo velocity and tympanometry in normal hearing adults, Ear Hear. 33 (2012) 19.
[65] X. Li, X. Hao, M. Zhao, Y. Wu, J. Yang, Y. Tian, G. Qian, Exfoliation of hexagonal boron nitride by molten hydroxides, Adv. Mater. 25 (2013) 2200–2204.
[66] X. Wang, Z. Chen, Z. Shen, Dynamic behavior of polymer surface and the time dependence of contact angle, Sci. China, Ser. B: Chem. 48 (2005) 553–559.
[67] B. Zhang, N. De Alwis Watuthanthrige, S. V Wanasinghe, S. Averick, D. Konkolewicz, Complementary dynamic chemistries for multifunctional polymeric materials, Adv. Funct. Mater. 32 (2022) 2108431.
[68] X. Shen, Q. Zheng, J.-K. Kim, Rational design of two-dimensional nanofillers for polymer nanocomposites toward multifunctional applications, Prog. Mater. Sci. 115 (2021) 100708.
[69] Y. Liao, C.-H. Loh, M. Tian, R. Wang, A.G. Fane, Progress in electrospun polymeric nanofibrous membranes for water treatment: fabrication, modification and applications, Prog. Polym. Sci. 77 (2018) 69–94.
[70] M. Milazzo, G.S. Jung, S. Danti, M.J. Buehler, Wave propagation and energy dissipation in collagen molecules, ACS Biomater. Sci. Eng. 6 (2020) 1367–1374, https://doi.org/10.1021/acsbiomaterials.9b01742.
[71] I. Kuru, H. Maier, M. Müller, T. Lenarz, T.C. Lueth, A 3D-printed functioning anatomical human middle ear model, Hear. Res. 340 (2016) 204–213.
[72] E.D. Kozin, N.L. Black, J.T. Cheng, M.J. Cotler, M.J. McKenna, D.J. Lee, J.A. Lewis, J.J. Rosowski, A.K. Remenschneider, Design, fabrication, and in vitro testing of novel three-dimensionally printed tympanic membrane grafts, Hear. Res. (2016), https://doi.org/10.1016/j.heares.2016.03.005.